Controlling exciton decay dynamics in semiconducting single-walled carbon nanotubes by surface acoustic waves

Markus Egid Regler, Hubert J. Krenner, A. A. Green, M. C. Hersam, Achim Wixforth, A. Hartschuh

Angaben zur Veröffentlichung / Publication details:

Regler, Markus Egid, Hubert J. Krenner, A. A. Green, M. C. Hersam, Achim Wixforth, and A. Hartschuh. 2013. "Controlling exciton decay dynamics in semiconducting single-walled carbon nanotubes by surface acoustic waves." *Chemical Physics* 413: 39–44. https://doi.org/10.1016/j.chemphys.2012.10.014.

Controlling exciton decay dynamics in semiconducting single-walled carbon nanotubes by surface acoustic waves

M.E. Regler [a,b], H.J. Krenner [b,c], A.A. Green [d], M.C. Hersam [d], A. Wixforth [b,c], A. Hartschuh [a,b,*]

[a] Department Chemie, Ludwig-Maximilians-Universität München, 81377 München, Germany
[b] CeNS, Ludwig-Maximilians-Universität München, 81377 München, Germany
[c] Lehrstuhl für Experimentalphysik 1 and Augsburg Centre for Innovative Technologies (ACIT), Universität Augsburg, Universitätstr. 1, 86159 Augsburg, Germany
[d] Department of Materials Science and Engineering, Department of Chemistry, Northwestern University, Evanston, IL 60208-3108, USA

ARTICLE INFO

Keywords:
Single-walled carbon nanotubes
Surface acoustic waves
Exciton decay dynamics

ABSTRACT

We show that the photoluminescence intensity and decay dynamics of semiconducting single-walled carbon nanotube films can be remotely controlled by surface acoustic waves (SAW) launched on the piezoelectric substrate $LiNbO_3$. Time-resolved measurements in the picosecond regime reveal that photoluminescence quenching results from a decrease of the radiative recombination rate by up to 25% for the accessible SAW amplitudes. The SAW-induced piezoelectric field acts as a quasi-static perturbation that polarizes the luminescent exciton state reducing the oscillator strength of the radiative transition following a quadratic field dependence. Surface acoustic waves could be used for the remote and contact-free electrical control of high-speed electronic and optoelectronic nanotube-based devices.

The direct band gap of semiconducting single-walled carbon nanotubes (SWCNTs) is of unique interest for the implementation of optical and electronic devices or sensors on the same material [1–4]. On this scalable, quasi one-dimensional platform, the successful realization of voltage-controlled light emission [5] and detection [6,7] and the demonstration of quantum light emission [8] represented major advances towards this goal. A key requirement to fully exploit the application potential of SWCNT is the ability to control their optical emission and absorption properties by easily accessible external parameters. Here, electric fields applied by an external voltage have shown to be particularly suitable, which in most cases however, require time and cost-intensive elaborate nano-contacting [9,1] of the nanotubes.

In the broad field of established and novel semiconductor-based nanostructures surface acoustic waves (SAW) have proven to be an extremely versatile tool to control and probe the electronic [10–12], optical [13–18] and photonic [19,20] properties of these nanosystems over macroscopic length scales and distances at frequencies ranging from a few megahertz up to several gigahertz. This unique property is based on the almost dissipation-free propagation of these radio frequency (rf) acousto-mechanical waves on the surface of solids over distances of several millimeters at the speed of sound (c_{sound}). Thus, a SAW pulse can interact with all nanosystems within its propagation path providing a unique tool for direct massively parallel addressing and manipulation. Moreover, these SAWs can be generated all-electrically, either directly on piezoelectric substrates [21] or on arbitrary substrates using piezoelectric coupling layers [22] using interdigital transducer electrodes (IDTs) with a lithographically defined periodicity p. By applying an rf voltage to the IDT with a frequency matching the dispersion relation of a SAW $f_{rf} = f_{\mathrm{SAW}} = c_{\mathrm{sound}}/2p$, a SAW of wavelength $\lambda_{\mathrm{SAW}} = 2p$ is launched. Such SAW chips are not limited to commercialized applications such as rf filtering in mobile communication devices [23,24] or SAW driven microfluidics [25], but can be directly hybridized with other types of nanosystems such as nanowires and nanotubes to study their optical [26] and electrical transport [27–29] properties.

In contrast to conventional semiconductors, for which the alternating electric fields induced by the SAW are sufficient to fully dissociate excitons, transport and inject the individual charge carriers [13,15,30,31,26], the strongly bound and short-lived excitons in SWCNT [32] are an ideal system to study the impact of a SAW representing a weak and quasi-static perturbation. Here, we show that the strong electrical fields associated with SAWs can be used to efficiently suppress or enhance the PL emission of a SWCNT film despite of the more than one order of magnitude larger exciton binding energies compared to semiconductor based systems. Furthermore, we apply time-resolved spectroscopy to directly confirm that the observed quenching of the SWCNT emission arises from a reduction of the radiative recombination rate of excitons interacting with the SAW-induced electric fields.

* Corresponding author at: Department Chemie, Ludwig-Maximilians-Universität München, 81377 München, Germany.
E-mail address: achim.hartschuh@cup.uni-muenchen.de (A. Hartschuh).

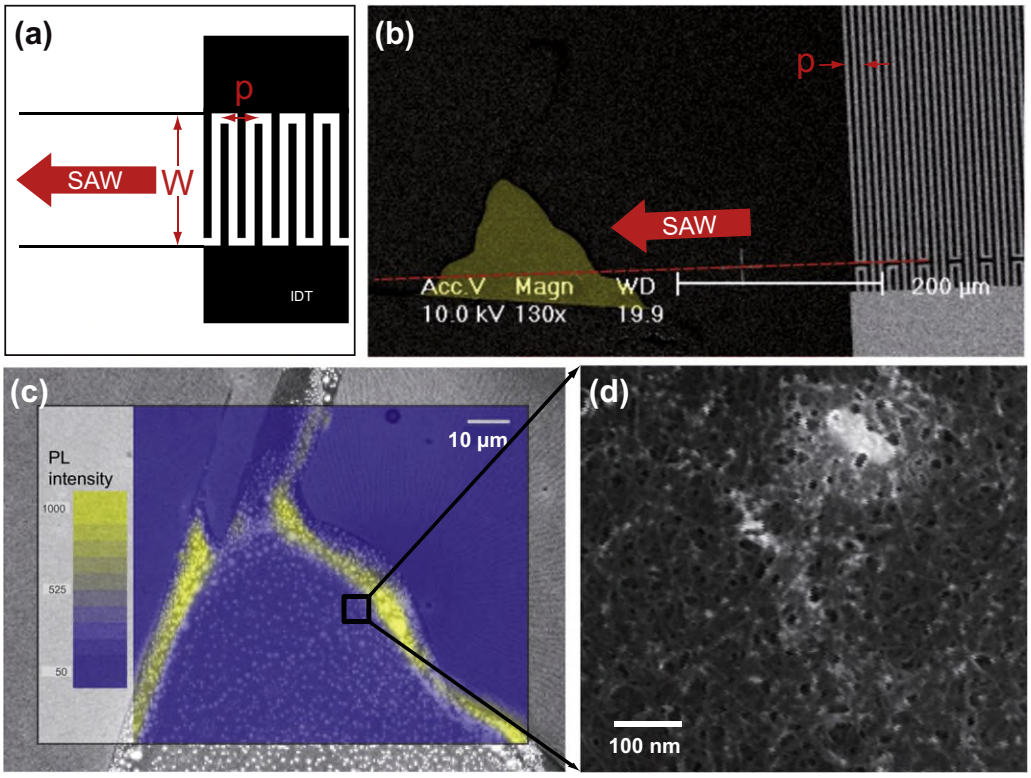

Fig. 1. (a) Schematic of the experimenal configuration used for the remote control of exciton decay in SWCNT. The samples are based on the piezoelectric substrate $LiNbO_3$. Interdigital transducers (IDT) with varying periodicities p were fabricated on the surface by standard optical lithography in order to launch surface acoustic waves. Drop-casting a SWCNT solution resulted in carbon nanotube films after drying. (b) Large area SEM image illustrating the IDT and the propagation direction of the SAW. (c) Magnified view of the area shaded yellow in (b). The corresponding PL intensity image is super-imposed onto the SEM image. The PL intensity is strongest in regions with very high SWCNT coverage. (d) Magnified view of the area marked by the square in (c) featuring a dense SWCNT network that has been used for the following measurements.

For our experiments we fabricated hybrid SWCNT-SAW devices consisting of a strongly piezoelectric lithium niobate ($LiNbO_3$) chip and a thin film of SWCNT (Fig. 1). On the $LiNbO_3$ substrate a set of different IDTs are fabricated which allow for SAW generation. Details on the IDT design and fabrication can be found in the Supporting information of this paper. For the experiments presented in this manuscript we used the IDT marked in the micrograph operating at a frequency of $f_{SAW} = 121$ MHz. An aqueous solution of CoMoCAT-SWCNTs wrapped by single-stranded DNA was dripped onto the chip surface in the propagation path of the SAW. This material contains mainly thin diameter nanotubes dominated by the species (6,4) and (6,5) [33–35]. A scheme illustrating the experimental configuration is shown in Fig. 1(a) together with a series of SEM images of the sample with increasing magnification (Fig. 1(b–d)). The magnified view of the area marked by the black square in Fig. 1(c) shown in (d) reveals a dense but rather uniform coverage of the surface with SWCNTs. The PL intensity measured for this sample is superimposed on the SEM image in Fig. 1(c). Strong PL is observed for high SWCNT coverage. The PL data presented in this paper were recorded in the area shown in Fig. 1(d). PL detection on $LiNbO_3$ substrates is hindered by the high refractive index of the material resulting in dominant radiation into the substrate. Thus, detection of single nanotube PL is not feasible with standard glass microscope objectives.

Nanotube PL was studied using a confocal raster scanning microscope with laser excitation at 565 nm or 800 nm. The PL signal was detected by an avalanche photo diode (APD) after passing spectral filters to select nanotube PL. A narrow bandpass filter transmitting at $\lambda = 980$ nm ± 10 nm was used to select the PL emitted from (6,5)-nanotubes, whereas light from both (6,5)- and (6,4)-nanotubes was detected using a 863 nm long pass filter. PL spectra were recorded by a spectrometer coupled to a CCD camera. Time-traces recorded in the second to microsecond regime allowed for the direct investigation of the influence of the SAW on the PL. High laser intensities were found to lead to an exponential decrease of the PL intensity due to photo-oxidation [36]. The PL time-traces recorded while varying the SAW amplitude were recorded at the lowest possible excitation intensities and corrected for residual PL bleaching by subtracting a single exponential decay contribution. Blinking events, presumably related to oxygen adsorption from air, were occasionally observed on the time-scale of seconds [36]. Repeated PL intensity measurements were carried out to distinguish SAW-induced effects. The decay dynamics of excitons in the picosecond range was observed using time-correlated single photon (TCSPC). Pulsed laser excitation at 800 nm was provided by a Ti:Sa-oscillator with a pulse duration of about 150 fs and a repetition rate of 76 MHz. Exciton lifetimes were determined by fitting the measured PL transients using exponential decay functions convoluted with the independently determined instrument response function [37]. In all experiments SAWs were generated using a conventional rf signal generator with a maximum output power of 200 mW.

In Fig. 2(a) a typical PL spectrum of the sample is shown featuring two emission bands centered at 890 nm and 990 nm identified as (6,4) and (6,5) nanotube emission, respectively. After the rf signal is switched on at $f_{rf} = 121$ MHz (excitation power $P = 200$ mW) the PL intensity is reduced uniformly by about 30% by the generated SAW. To unambiguously prove that this effect indeed arises from the SAW we keep the applied rf power constant and scan the applied frequency through the resonance of the IDT. In the normalized PL intensity $\Delta I = I^{SAW}(f)/I^0$ presented in Fig. 2(b) we observe a pronounced minimum at the design frequency of the IDT

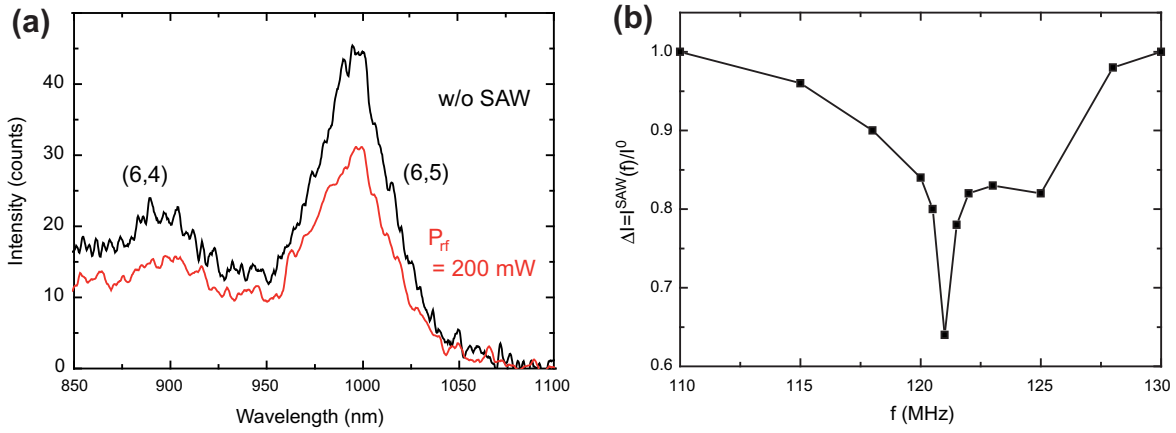

Fig. 2. (a) PL spectrum of the nanotube network on $LiNbO_3$ showing contributions from (6,5) and (6,4) SWCNTs at 990 nm and 890 nm, respectively. In the presence of the SAW the PL intensity is reduced substantially (red line) while no significant spectral shifts are observed. (b) Dependence of the normalized PL intensity $\Delta I = I^{SAW}(f)/I^0$ on the driving frequency f of the IDT. Quenching of the nanotube PL intensity occurs only within the resonance frequency of the IDT $f_{SAW} = 121$ MHz.

of $f_{SAW} = 121$ MHz. For detuned frequencies no pronounced variation of the PL intensity is observed. This clearly shows that the PL intensity is connected to the SAW amplitude that is most efficiently excited at the IDT's resonance frequencies.

The detailed dependence of the PL intensity on the power of the SAW was measured in a time-series shown in Fig. 3(a). We switch on a continuous wave rf signal at different power levels for $\delta t \sim 100$ s followed by a break of about the same duration. We start at the maximum rf power of 200 mW and observe a strong suppression of the normalized PL intensity to $\Delta I = I^{SAW}(f)/I^0 = 0.7$ consistent with the data shown Fig. 2. As we decrease P_{rf} the contrast in the PL intensity reduces continuously and vanishes at ~ 0 mW. Over the total duration of the experiment of almost 3000 s we do not observe pronounced photobleaching effects as ΔI recovers to ~ 1 after each step. This data clearly demonstrates reversible on-off switching of the SWCNT emission while the contrast of the modulation is directly correlated to the SAW power. For a more detailed analysis we extract ΔI from this data and plot it as a function of P_{rf} which is shown in Fig. 3(b). We resolve a clear linear dependence of ΔI on the applied rf power. Since the amplitude of the electric field F induced by the SAW is proportional to $\sqrt{P_{rf}}$, our experimental data suggests a quadratic dependence of the PL suppression on F. For further analysis we thus convert P_{rf} to the corresponding electric field (F) for a given substrate and IDT geometry (additional details in Supporting information).

For static fields quenching of carbon nanotube photoluminescence has been reported in [38]. The dependence of the PL intensity on the field amplitude was modeled by a hyperbolic cosine function. The two exponential terms with opposite sign contained in $\cosh(x) = (\exp(x) + \exp(-x))/2$ were discussed to result from two processes affecting the non-radiative exciton decay rate in opposite ways: one increasing the non-radiative decay from its zero-field value while the other decreasing it. An interpretation involving increased exciton dissociation as the origin of non-radiative rate-enhancement was given. Using this model the PL intensity variation is described by

$$\Delta I = \cosh(h \cdot F)^{-1} \tag{1}$$

with h being an empirical parameter representing the sensitivity of the PL intensity to the applied electric field.

Complete dissociation, i.e., field-induced ionization of E_{11} excitons into single-particle states, appears to be unlikely in our experiments due to the huge exciton binding energies of the present thin-diameter nanotubes of about 400 meV. Following the discussion in [39] we estimate an extremely low exciton dissociation rate of $\sim 10^{-50}$ eV for (6,5) nanotubes at the maximum electric field of $F \approx 4$ V/μm accessible in our experiment. A second-order perturbative treatment of the electric field effect, in analogy to the quadratic Stark effect in the case of the hydrogen atom or an exciton in semiconductors, on the other hand, predicts the transfer of

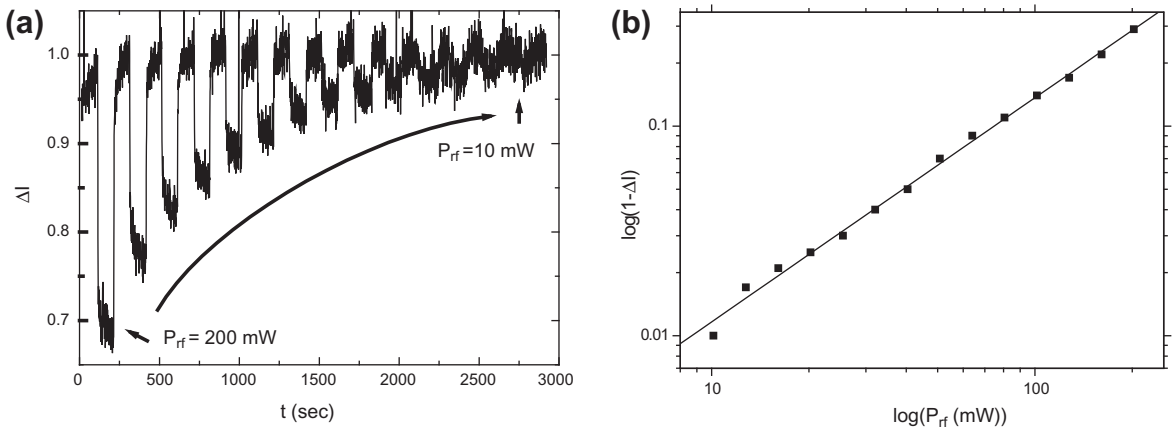

Fig. 3. (a) SAW power dependence of the PL intensity $\Delta I = I^{SAW}/I^0$ observed by switching the SAW on and off while varying the rf power P_{rf} at the IDT resonance frequency. The rf amplitude varied from 200 mW to 10 mW. The relative intensity ΔI decreases reversibly with increasing power. (b) Relative PL intensity vs. SAW power P_{rf}. The solid line is a linear fit.

spectral weight from the exciton transition towards band-to-band transitions [39]. This decrease of the oscillator strength, a consequence of the reduced overlap between electron and hole components of the exciton wavefunction, results in a reduction of the radiative recombination rate and thus in a decreased PL intensity. Such electric field driven control of the electron-hole separation has been demonstrated for different semiconductor quantum dot nanostructures over the past 10 years [40–45].

Both field-induced processes, non-radiative rate enhancement and radiative rate reduction, would lead to lower PL intensities and cannot be distinguished in a time-integrated experiment. However, since the former would lead to faster exciton decay times whereas the latter to slower ones both phenomena can be clearly distinguished by time-resolved PL measurements.

PL transients measured after femtosecond laser pulse excitation with and without SAW are presented in Fig. 4(a). From the measured PL transients we extract a monoexponential decay with an exciton lifetime of ~ 6.8 ps after deconvolution of the instrument response function. This value is somewhat shorter compared to results obtained for individual SWCNTs of the same material deposited on glass but close to ensemble values [32,37,46]. This shortening is expected due to nanotube-nanotube interactions within the network and the stronger radiative coupling to the $LiNbO_3$ substrate that features a higher refractive index than glass, about 2.3 vs. 1.5. Giving both, the SAW period of ~8 ns being three orders of magnitudes longer than the PL decay time and the large exciton binding energies, the SAW-induced electrical fields can be considered to be a weak, quasi-static perturbation within the exciton lifetime.

In the presence of the SAW we observe a decrease of the maximum intensity of the transient confirming our previous observations shown in Fig. 3. In addition we resolve a clear increase of the exciton lifetime by ~15% to about 7.8 ps. Although the observed effect is small when compared to semiconductor heterostructures [15,47] with small exciton binding energies, it is highly reproducible and supported by the clear correlation seen in Fig. 4(b) for increasing SAW power. Most importantly, all transients measured to obtain the data shown in Fig. 4(b) were taken from the same sample position and for the same excitation and detection conditions while only varying the amplitude of the rf signal that generates the SAW. We therefore can exclude influences from sample heterogeneities and variations in the optical alignment as giving rise to the observed effect. The error bars given in Fig. 4(b) reflect the absolute error that is determined by the temporal width of the measured instrument response function of 27 ps. The relative error, which is the essential quantity for the following discussion of the relative radiative rate modifications, is substantially smaller as can be seen from the spread of the three data points at $P_{rf} = 0$ mW. Measurement series for other sample positions revealed the same SAW-induced slowdown of exciton decay, albeit with slightly varying absolute exciton lifetimes that can be expected for a nanotube film [32]. Thus we conclude that the time-resolved data clearly show that the exciton lifetime increases continuously with increasing electric field strength. The observed exciton lifetime τ results from the sum of the radiative k_{rad} and non-radiative decay k_{nonrad} rates adding up to the total PL decay rate $\tau^{-1} = k_{\mathrm{rad}} + k_{\mathrm{nonrad}}$. We exclude an increase of non-radiative contributions as the dominating contribution since such processes would lead to faster total exciton decay.

Using the experimental data we can calculate the modification of the radiative rate Δk induced by the SAW. The total PL intensity I can be calculated from the initial number of excitons N and the PL quantum yield $Q = k_{\mathrm{rad}}\tau$ according to $I = \eta NQ = \eta N k_{\mathrm{rad}}\tau$. Here η considers the detection sensitivity of the setup. Forming the ratio between PL intensities $\Delta I = I^{\mathrm{SAW}}/I^{0}$ we obtain $\Delta I \approx \Delta k_{\mathrm{rad}}\Delta\tau$ using $\Delta k_{\mathrm{rad}} = k_{\mathrm{rad}}^{\mathrm{SAW}}/k_{\mathrm{rad}}^{0}$ and $\Delta\tau = \tau^{\mathrm{SAW}}/\tau^{0}$. Here we neglect changes in the excitation rate and use the approximation $\Delta N = N^{\mathrm{SAW}}/N^{0} \approx 1$. The electric field transfers oscillator strength from the exciton to the free-carrier absorption as described in Ref. [39]. Reduced exciton absorption could thus be balanced partially by increased free-carrier absorption depending on the excitation energy. In fact, SAW-controlled PL intensity measurements for resonant excitation at 565 nm, matching the E_{22} exciton energy of both nanotube species (6,5) and (6,4) studied here and non-resonant excitation at 800 nm revealed no significant differences. Relative changes in the radiative rate can then be calculated from experimental data obtained within the same measurement according to $\Delta k_{\mathrm{rad}} \approx \Delta I/\Delta\tau$.

In Fig. 5(a) Δk_{rad} is plotted vs. the electric field F. The radiative rate decreases continuously for increasing field strength and is reduced by up to 25%. The radiative rate is proportional to the oscillator strength f of the exciton transition which scales with the

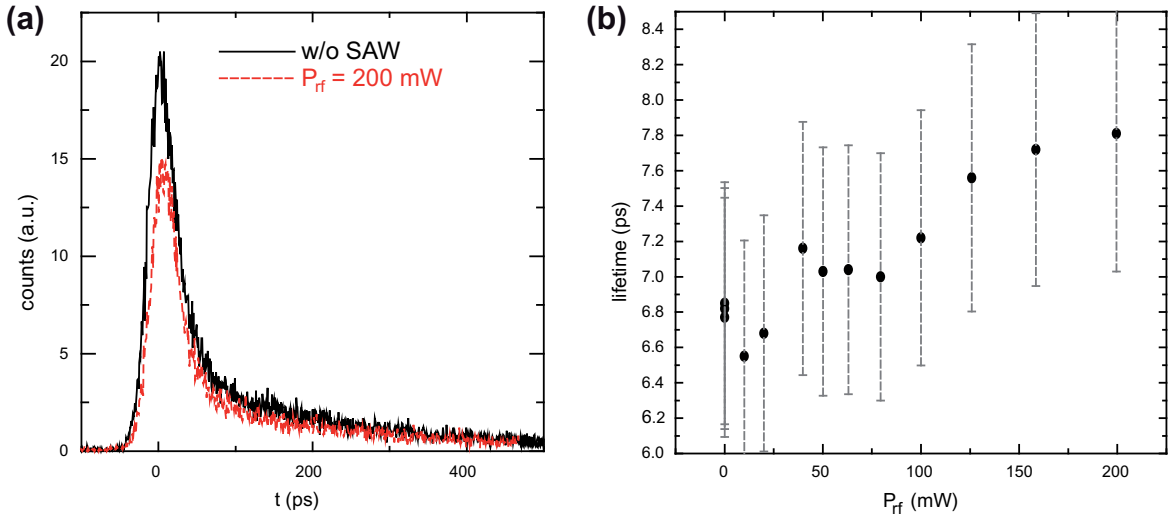

Fig. 4. Influence of the surface acoustic wave on the exciton decay. (a) Time-resolved PL decay measured at the same sample position with and without SAW. Besides a strong amplitude reduction a small increase in the temporal width of the PL transient is observed. (b) Exciton lifetimes determined from PL transients measured at the same sample position while varying the power of the SAW. A systematic increase of the exciton lifetime is observed for increasing SAW power. Since the PL intensity decreases at the same time, (b) evidences a decrease of the radiative decay rate of the exciton.

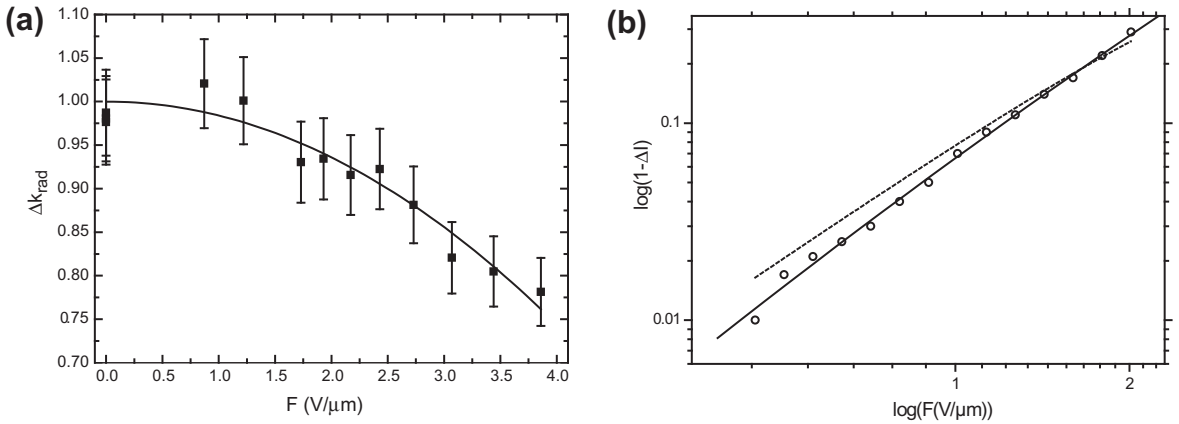

Fig. 5. (a) Electric field-dependence of the radiative rate calculated from the decay measured in 4 and the simultaneously determined PL intensity. The sold line is a model function based on the quadratic Stark effect reducing electron-hole overlap.(b Field dependence of the PL intensity from 3(b). The solid line is a fit based on radiative rate reduction $\Delta I \approx 1 - \kappa' F^2$. The dashed line is a fit 1 assuming two competing field-controlled processes.

squared modulus of the overlap integral of electron and hole wavefunctions. Within second-order perturbation theory the oscillator strength decreases quadratically with the applied electric field F and we thus find

$$\Delta k_{\mathrm{rad}} \approx (f - \kappa F^2)/f = 1 - \kappa' F^2, \tag{2}$$

where κ and κ' are scaling factors. The observed field dependence of the radiative rate can be well described by the derived relation as can be seen from the fit in Fig. 5(a) (solid line).

Having identified radiative rate reduction as the main origin for the PL reduction, we can now also model the PL data from Fig. 3(b) that is shown in Fig. 5(b) as a function of the electric field. The solid line is a fit following $\Delta I \propto \Delta k_{\mathrm{rad}} \approx 1 - \kappa' F^2$ by neglecting changes in the lifetime. For comparison we included a fit by an inverse cosh function (1), dashed line in Fig. 5(b), that would imply two competing processes with opposite effects. While the fit based on Eq. (1) reproduces the general trend, systematic deviations from the measured data are apparent. In contrast, the good agreement between the experimental data and the fit using Eq. (2) clearly supports our interpretation for the present system and electric field amplitudes.

As a result we have shown that both nanotube PL intensity and lifetime can be used to probe the local electric field strength. More detailed investigations of the PL intensity indicate that the electric fields within the SWCNT network on $LiNbO_3$ are not constant in time. PL intensity traces on shorter time-scales show a first instantaneous and a second slower response to SAW-switching (Fig. 6(a)). After the fast PL decrease a slower decay of the PL intensity that amounts to about 20% of the total contrast is observed within several tens of seconds. A similar delayed response is seen after the SAW has been switched off. From this we conclude that the nanotubes are not exposed only to the instantaneous field provided by the SAW, but also sense a slower SAW-induced buildup of a polarization field that is probably formed by the redistribution of mobile charge carriers in residual charged DNA molecules on the sample surface used for SWCNT solubilization or also within the SWCNT network. The presence of local quasi-static fields related to charges on the substrate would also be expected to modify the PL intensity and the exciton oscillator strength following the observations made above. In fact, in several cases the SAW was seen to increase the PL intensity (Fig. 6(b)). This can be understood in terms of SAW-induced fields partially compensating existing local fields or removing trapped charges as observed for example for semiconductor quantum dots [17].

We note that at the maximum excitation power used in the experiment to excite the SAW sample heating on the order of 10 K can be expected. Experimental and theoretical studies on

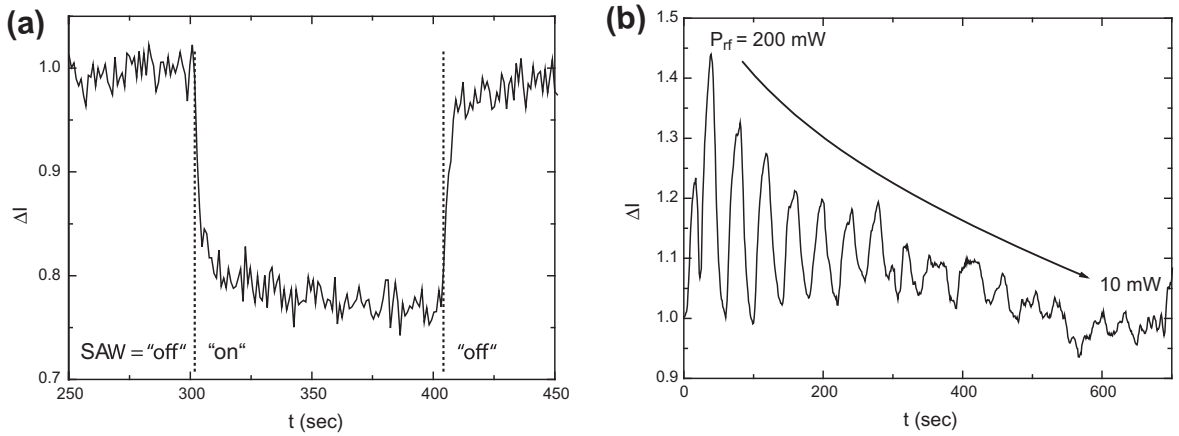

Fig. 6. (a) Response of the PL intensity to SAW-switching. Besides the instantaneous decrease that dominates the response, a slower decay on the time-scale of several seconds is observed. A comparable delayed response occurs also after switch-off. The delayed response is attributed to a slow polarization of the DNA-SWCNT network on the sample surface by mobile charge carriers that create local static fields. (b) SAW power dependence of the PL intensity $\Delta I = I^{\mathrm{SAW}}/I^0$ recorded by switching the SAW on and off while varying the rf power P_{rf} following the same procedure as described in Fig. 3(a) for a different sample position. At some spots on the sample, about 10% of observed cases, the PL intensity increases with the SAW. This can be understood in terms of localized quasi-static fields that are partially compensated by the SAW-induced fields.

the PL intensity and radiative decay rate of thin diameter SWCNTs revealed that at around 295 K both quantities depend only weakly on the sample temperature [48–51]. SAW-related heating of the nanotubes is thus not likely to contribute substantially to the observed PL quenching and decrease in radiative rate. Contributions of temperature variations to the slow response on the time scale of several tens of seconds observed in Fig. 6 cannot be excluded.

In summary, we have shown that surface acoustic waves can be used to remotely control the photoluminescence intensity in semiconducting single-walled carbon nanotubes. The electric field associated with the SAW is found to slowdown exciton decay by reducing the radiative recombination rate. Time-resolved photoluminescence measurements show a quadratic field dependence of the relative radiative rate reduction. In contrast to most inorganic semiconductor nanostructures and materials, such as quantum dots or wells, field-induced exciton dissociation can be neglected for accessible SAW-related field amplitudes due to the large exciton binding energies of thin-diameter SWCNTs.

Acknowledgement

This work was supported by the Deutsche Forschungsgemeinschaft (DFG) through the Nanosystems Initiative Munich (NIM) and HA4405/4-1. HJK acknowledges support by the DFG via the Emmy Noether Program (KR3790/2-1). MCH acknowledges support by the National Science Foundation (DMR-1006391 and DMR-1121262) and the Nanoelectronics Research Initiative.

Appendix A. Supplementary data

Supplementary data associated with this article can be found, in the online version, at http://dx.doi.org/10.1016/j.chemphys.2012.10.014.

References

[1] P. Avouris, M. Freitag, V. Perebeinos, Nature Photon. 2 (2008) 341.
[2] M. Engel, J.P. Small, M. Steiner, M. Freitag, A.A. Green, M.C. Hersam, P. Avouris, ACS Nano 2 (2008) 2445.
[3] M. Kinoshita, M. Steiner, M. Engel, J.P. Small, A.A. Green, M.C. Hersam, R. Krupke, E.E. Mendez, P. Avouris, Opt. Exp. 18 (2010) 25738.
[4] L. Cognet, D.T. Tsyboulski, J.-D.R. Rocha, C.D. Doyle, J.M. Tour, R.B. Weisman, Science 316 (2007) 1465.
[5] J. Chen, V. Perebeinos, M. Freitag, J. Tsang, Q. Fu, J. Liu, P. Avouris, Science 310 (2005) 1171.
[6] M. Freitag, Y. Martin, J.A. Misewich, R. Martel, P. Avouris, Nano Lett. 3 (2003) 1067.
[7] N.M. Gabor, Z. Zhong, K. Bosnick, J. Park, P.L. McEuen, Science 325 (2009) 1367.
[8] A. Högele, C. Galland, M. Winger, A. Imamoğlu, Phys. Rev. Lett. 100 (2008) 217401.
[9] P. Avouris, Z. Chen, V. Perebeinos, Nature Nanotechnol. 2 (2007) 605.
[10] A. Wixforth, J. Scriba, M. Wassermeier, J.P. Kotthaus, G. Weimann, W. Schlapp, Phys. Rev. B 40 (1989) 7874.
[11] M. Rotter, A.V. Kalameitsev, A.O. Govorov, W. Ruile, A. Wixforth, Phys. Rev. Lett. 82 (1999) 2171.
[12] I.V. Kukushkin, J.H. Smet, V.W. Scarola, V. Umansky, K. von Klitzing, Science 324 (2009) 1044.
[13] C. Rocke, S. Zimmermann, A. Wixforth, J.P. Kotthaus, G. Böhm, G. Weimann, Phys. Rev. Lett. 78 (1997) 4099.
[14] P.V. Santos, M. Ramsteiner, F. Jungnickel, Appl. Phys. Lett. 72 (1998) 2099.
[15] A. García-Cristóbal, A. Cantarero, F. Alsina, P.V. Santos, Phys. Rev. B 69 (2004) 205301.
[16] J.R. Gell, M.B. Ward, R.J. Young, R.M. Stevenson, P. Atkinson, D. Anderson, G.A.C. Jones, D.A. Ritchie, A.J. Shields, Appl. Phys. Lett. 93 (2008) 081115.
[17] S. Völk, F.J.R. Schülein, F. Knall, D. Reuter, A.D. Wieck, T.A. Truong, H. Kim, P.M. Petroff, A. Wixforth, H.J. Krenner, Nano Lett. 10 (2010) 3399.
[18] A. Hernández-Mínguez, M. Möller, S. Breuer, C. Pfüller, C. Somaschini, S. Lazić, O. Brandt, A. García-Cristóbal, M.M. de Lima, A. Cantarero, L. Geelhaar, H. Riechert, P.V. Santos, Nano Lett. 12 (2012) 252.
[19] M.M. de Lima Jr., P.V. Santos, Rep. Progr. Phys. 68 (2005) 1639.
[20] D.A. Fuhrmann, S.M. Thon, H. Kim, D. Bouwmeester, P.M. Petroff, A. Wixforth, H.J. Krenner, Nature Photon. 5 (2011) 605.
[21] R.M. White, F.W. Voltmer, Appl. Phys. Lett. 7 (1965) 314.
[22] S. Ono, O. Yamazaki, K. Ohji, K. Wasa, S. Hayakawa, Appl. Phys. Lett. 33 (1978) 217.
[23] S. Datta, Surface Acoustic Wave Devices, Prentice Hall, Englewood Cliffs, NJ, 1986 (1986).
[24] C.K. Campell, Surface Acoustic Wave Devices for Mobile and Wireless Communications, Academic Press, San Diego, CA, 1998 (1998).
[25] A. Wixforth, Superlatt. Microstruct. 33 (2003) 389.
[26] J.B. Kinzel, D. Rudolph, M. Bichler, G. Abstreiter, J.J. Finley, G. Koblmüller, A. Wixforth, H.J. Krenner, Nano Lett. 11 (2011) 1512.
[27] C. Würstle, J. Ebbecke, M.E. Regler, A. Wixforth, New J. Phys. 9 (2007) 73.
[28] B.K. Kim, J.J. Kim, M. Seo, Y. Chung, B.C. Woo, J. Kim, W. Song, N. Kim, Appl. Phys. Lett. 97 (2010) 262110.
[29] S. Roddaro, E. Strambini, L. Romeo, V. Piazza, K. Nilsson, L. Samuelson, F. Beltram, Semicond. Sci. Technol. 25 (2010) 024013.
[30] O.D.D.J. Couto, S. Lazic, F. Iikawa, J.A.H. Stotz, U. Jahn, R. Hey, P.V. Santos, Nature Photon 3 (2009) 645.
[31] S. Völk, F. Knall, F.J.R. Schülein, T.A. Truong, H. Kim, P.M. Petroff, A. Wixforth, H.J. Krenner, Appl. Phys. Lett. 98 (2011) 023109.
[32] T. Gokus, L. Cognet, J.G. Duque, M. Pasquali, A. Hartschuh, B. Lounis, J. Phys. Chem. C 114 (2010) 14025.
[33] M. Zheng, A. Jagota, E.D. Semke, B.A. Diner, R.S. Mclean, S.R. Lustig, R.E. Richardson, N.G. Tassi, Nat. Mater. 2 (2003) 338.
[34] M.S. Arnold, A.A. Green, J.F. Hulvat, S.I. Stupp, M.C. Hersam, Nature Nanotechnol. 1 (2006) 60.
[35] A.A. Green, M.C. Hersam, Adv. Mater. 23 (2011) 2185.
[36] C. Georgi, N. Hartmann, T. Gokus, A.A. Green, M.C. Hersam, A. Hartschuh, Chem. Phys. Chem. 9 (2008) 1460.
[37] T. Gokus, H. Harutyunyan, F. Hennrich, P.T. Araujo, M. Kappes, A. Jorio, A.A. Green, M.C. Hersam, M. Allegrini, A. Hartschuh, Appl. Phys. Lett. 92 (2008) 153116.
[38] A.V. Naumov, S.M. Bachilo, D.A. Tsyboulski, R.B. Weisman, Nano Lett. 8 (2008) 1527.
[39] V. Perebeinos, P. Avouris, Nano Lett. 7 (2007) 609.
[40] P.W. Fry, I.E. Itskevich, D.J. Mowbray, M.S. Skolnick, J.J. Finley, J.A. Barker, E.P. O'Reilly, L.R. Wilson, I.A. Larkin, P.A. Maksym, M. Hopkinson, M. Al-Khafaji, J.P.R. David, A.G. Cullis, G. Hill, J.C. Clark, Phys. Rev. Lett. 84 (2000) 733.
[41] H.J. Krenner, M. Sabathil, E.C. Clark, A. Kress, D. Schuh, M. Bichler, G. Abstreiter, J.J. Finley, Phys. Rev. Lett. 94 (2005) 057402.
[42] R.M. Kraus, P.G. Lagoudakis, A.L. Rogach, D.V. Talapin, H. Weller, J.M. Lupton, J. Feldmann, Phys. Rev. Lett. 98 (2007) 017401.
[43] T. Nakaoka, E.C. Clark, H.J. Krenner, M. Sabathil, M. Bichler, Y. Arakawa, G. Abstreiter, J.J. Finley, Phys. Rev. B 74 (2006) 121305.
[44] H.J. Krenner, C.E. Pryor, J. He, P.M. Petroff, Nano Lett. 8 (2008) 1750.
[45] K.C. Wijesundara, J.E. Rolon, S.E. Ulloa, A.S. Bracker, D. Gammon, E.A. Stinaff, Phys. Rev. B 84 (2011) 081404.
[46] Z. Zhu, J. Crochet, M.S. Arnold, M.C. Hersam, H. Ulbricht, D. Resasco, T. Hertel, J. Phys. Chem. C 111 (2006) 3831.
[47] T. Sogawa, H. Sanada, H. Gotoh, H. Yamaguchi, S. Miyashita, P.V. Santos, Appl. Phys. Lett. 94 (2009) 131912.
[48] V. Perebeinos, J. Tersoff, P. Avouris, Nano Lett. 5 (2005) 2495.
[49] C.D. Spartaru, S. Ismail-Beigi, R.B. Capaz, S.G. Louie, Phys. Rev. Lett. 95 (2005) 247402.
[50] I.B. Mortimer, R.J. a. Nicholas, Phys. Rev. Lett. 98 (2007) 027404.
[51] W.K. Metzger, T.J. McDonald, C. Engtrakul, J.L. Blackburn, G.D. Scholes, G. Rumbles, M.J. Heben, J. Phys. Chem. 111 (2007) 3601.